Depolarized Resonance Light Scattering by Porphyrin and Chlorophyll *a* Aggregates

Jai Parkash,* John H. Robblee,* John Agnew,* Esther Gibbs,# Peter Collings,§ Robert F. Pasternack,¶ and Julio C. de Paula*

*Department of Chemistry, Haverford College, Haverford, Pennsylvania 19041; #Department of Chemistry, Goucher College, Towson, Maryland 21204; and Departments of §Physics and Astronomy and ¶Chemistry, Swarthmore College, Swarthmore, Pennsylvania 19081 USA

ABSTRACT A quantum mechanical model is developed for the observed resonance enhancement of light scattering by aggregates of electronically interacting chromophores. Aggregate size, monomer oscillator strength, extent of electronic coupling, and aggregate geometry are all important determinants of intensity in resonance light scattering (RLS) spectra. The theory also predicts the value of the depolarization ratio ($\rho_V(90)$) of RLS for a given aggregate geometry. These results are used to interpret the RLS depolarization ratios of four aggregates: tetrakis(4-sulfonatophenyl)porphine aggregated at low pH ($\rho_V(90) = 0.17$ at 488 nm), *trans*-bis(N-methylpyridinium-4-yl)-diphenylporphinato copper(II) aggregated in 0.2 M NaCl solution ($\rho_V(90) = 0.13$ at 450 nm) and on calf thymus DNA ($\rho_V(90) = 0.20$ at 454 nm), and chlorophyll *a* aggregates in formamide/water ($\rho_V(90) = 0.23$ and 0.32 at 469 and 699 nm, respectively). The analysis is consistent with a J-aggregate geometry for all four systems. Furthermore, the specific values of $\rho_V(90)$ allow us to estimate the orientation of the monomer transition dipoles with respect to the long axis of the aggregate. We conclude that depolarized resonance light scattering spectroscopy is a powerful probe of the geometric and electronic structures of extended aggregates of strong chromophores.

INTRODUCTION

Recent studies have shown that a number of biological light-harvesting systems, such as the LHI and LHII complexes of purple photosynthetic bacteria (McDermott et al., 1995; Karrash et al., 1995; Cogdell et al., 1996; Pullerits and Sundström, 1996) and the chlorosome of green photosynthetic bacteria (Blankenship et al., 1995), consist of aggregated bacteriochlorophylls. These results have sparked renewed interest in the design and characterization of supramolecular assemblies of chromophores (Lehn, 1995)—most notably chlorophylls (Katz et al., 1991; Scherz et al., 1991) and the related porphyrins (Fuhrhop et al., 1994; Pasternack and Gibbs, 1996)—that mimic the energy transfer function of photosynthetic antenna complexes.

New spectroscopic techniques need to be developed to selectively and sensitively probe the rather unique electronic and geometric structures of supramolecular light-harvesting systems. Work from our laboratories suggests that a new light scattering technique, resonance light scattering (RLS), may be used to determine both ground and excited state structures of extended porphyrin (Pasternack et al., 1993, 1994; Pasternack and Collings, 1995) and chlorophyll aggregates (de Paula et al., 1995).

The RLS effect consists of an increase in the intensity of scattered light at the wavelength where the aggregate has an electronic absorption transition. The phenomenon, observed in a variety of systems such as semiconductors (Gurioli et al., 1996), small chromophores in solution (Anglister and Steinberg, 1979; Stanton et al., 1981), chromophore-protein complexes (Ma et al., 1996; Borissevitch et al., 1997), chromophore-nucleic acid complexes (Pasternack et al., 1993, 1996; Huang et al., 1997), porphyrin aggregates (Pasternack et al., 1993, 1994), and chlorophyll *a* aggregates (de Paula et al., 1995), is consistent with all known theories of light-matter interactions (Miller, 1978; Anglister and Steinberg, 1979; Stanton et al., 1981; Pasternack and Collings, 1995; Lagendijk and van Tiggelen, 1996). A number of studies have shown that supramolecular assemblies show RLS signals that are intense enough for detection with commercial spectrofluorimeters (Pasternack et al., 1993, 1994; de Paula et al., 1995; Ma et al., 1996, 1997; Huang et al., 1997). Detection of RLS by monomers and small oligomers requires special methods to correct for strong absorption effects at the resonance frequency (Anglister and Steinberg, 1979; Stanton et al., 1981; Borissevitch et al., 1997).

Pasternack and Collings (1995) have suggested that the RLS technique may be used to determine the size and shape of chromophore aggregates in much the same way that conventional steady-state and dynamic light scattering measurements yield the size and shape of biopolymers. However, this potential will be realized only when the quantum mechanical basis for the large RLS intensities in exciton-coupled systems (such as porphyrin and chlorophyll aggregates) have been described.

In this contribution we develop a theoretical model for resonance light scattering by exciton-coupled systems, with the goal of describing the dependence of RLS intensity on aggregate size, strength of electronic coupling, and aggregate geometry. The model allows for correlation of the

Received for publication 22 October 1997 and in final form 13 January 1998.

Address reprint requests to Prof. Julio C. de Paula, Department of Chemistry, Haverford College, Haverford, PA 19041. Tel.: 610-896-1217; Fax: 610-896-4904; E-mail: jdepaula@haverford.edu.

0006-3495/98/04/2089/11 $2.00

degree of depolarization of the RLS signal with the geometry of the aggregate. These principles are applied to depolarized resonance light scattering spectra of tetrakis(4-sulfonatophenyl)porphine ($H_2TPPS_4^{4-}$) aggregated at low pH, *trans*-bis(N-methylpyridinium-4-yl)-diphenylporphinato copper(II) aggregated in 0.2 M NaCl solution and on calf thymus DNA, and of chlorophyll *a* aggregates in formamide/water. The results indicate that depolarized resonance light scattering spectroscopy is a powerful probe of the geometric and electronic structures of extended aggregates of strong chromophores.

MATERIALS AND METHODS

Computer simulations of RLS by aggregates

All mathematical operations described in the Theory section were performed on a Dell Latitude LX 4100D notebook computer (486DX processor, 100 MHz clock, 12 Mb RAM) with MathCAD Plus version 5.0 (MathSoft). Copies of the files are available from Julio de Paula.

Depolarized resonance light scattering measurements

For vertically polarized exciting radiation and scattered radiation detected at 90°, the depolarization ratio is defined as $\rho_V(90) = I_{VH}/I_{VV}$, where I_{VH} is the scattered intensity with horizontal polarization and I_{VV} is the scattered intensity with vertical polarization. We have measured $\rho_V(90)$ with two instruments: a spectrofluorimeter and a laser light scattering apparatus.

The fluorimeters used were a SPEX Fluorolog 2 and a Fluorolog 3, both equipped with a xenon lamp, a 0.25-m excitation monochromator, a 0.34-m emission monochromator, a photomultiplier tube (PMT) operating in photon counting mode in the sample arm, and a photodiode detector in the reference arm. The spectral bandwidth for our measurements was 1.0 nm. Glan-Thompson linear polarizers were used to polarize the exciting beam and to analyze the scattered radiation. It is necessary to correct the value of I_{VH} for the polarization-dependent response of the emission monochromator. Hence, the measured quantity was

$$\rho_V(90) = G \cdot \frac{I_{VH}}{I_{VV}} \tag{1}$$

where $G = I_{HV}/I_{HH}$ is the correction factor. This is the same correction factor generally used to correct fluorescence anisotropy data obtained with spectrofluorimeters (Lakowicz, 1986).

The laser light scattering apparatus is a Brookhaven Instruments Corporation BI-200SM goniometer. The excitation source is a Coherent Innova 70 mixed-gas ion laser (argon ion and krypton ion). The exciting beam is vertically polarized. Scattered light detected at 90° relative to the excitation beam is passed first through a linear polarizer and then through a narrow bandpass filter (which allows only the Rayleigh scattered light to pass) before reaching the PMT detector.

Preparation of aggregates

Chlorophyll *a* aggregates in aqueous formamide solution were prepared according to de Paula et al. (1995). Briefly, a stock solution of chlorophyll *a* (from *Anacystis nidulans,* purchased from the Sigma Chemical Company, St. Louis, MO) in acetone (spectrophotometric grade, Aldrich Chemical Company, Milwaukee, WI) was prepared and its concentration determined spectrophotometrically by using $\epsilon_{661.6\ nm} = 82.6\ mM^{-1}\ cm^{-1}$. Enough stock solution was added to a 9:1 (v/v) solution of formamide (spectrophotometric grade, Aldrich Chemical Company, Milwaukee, WI) and 75 mM potassium phosphate buffer (pH 6.8) so that the final concentration of chlorophyll *a* was ~4.0 μM. Aggregates form within 2 h of incubation in the dark at 4°C.

Aggregates of tetrakis(4-sulfonatophenyl)porphine ($H_2TPPS_4^{4-}$, Midcentury Chemicals) were formed by adding a small aliquot (~ 25 μl) of a stock solution of porphyrin in deionized water to ~9 ml of 0.2 M HCl. Formation of the aggregate was confirmed by the appearance of a sharp electronic absorption band at 489 nm and by a strong RLS feature at 489 nm.

Porphyrin-DNA complexes were prepared from the Cu(II) derivative of *trans*-bis(N-methylpyridinium-4-yl)-diphenylporphine (CuP_{agg}^{2+}) and calf thymus DNA (lot number QC81456203, Pharmacia Fine Chemicals) according to Pasternack et al. (1993). Formation of the porphyrin aggregate on the DNA template was confirmed by absorption and CD spectroscopy. The samples for which data are reported were typically 55 μM in DNA, 4.8 μM in CuP_{agg}^{2+}, and 0.2 M in NaCl. The solvent was a 1-mM potassium phosphate buffer (pH 6.80). CuP_{agg}^{2+} was aggregated in 0.2 M aqueous NaCl solution to give a final $[CuP_{agg}^{2+}] = 1.94\ \mu M$.

THEORY

Exciton coupling in J-, H-, double-stranded, and cylindrical aggregates

The first step in the calculation of scattering cross-sections of aggregates in a variety of geometries is to determine the aggregate's transition frequencies and moments by exciton coupling theory. Then the wavelength dependence of the aggregate's polarizability is calculated, and from that the scattering cross-sections and depolarization ratios are determined.

Our exciton coupling calculations use the point dipole approximation, which has been somewhat successful in describing the photophysical properties of light-harvesting systems (Pearlstein, 1991). Each monomer is described by a single transition with transition moment μ_{mon} and frequency $\tilde{\nu}_{mon}$. We will treat five coupling geometries, shown in Fig. 1.

The geometries of Fig. 1 *a* correspond to the well-known J-aggregates ($0 \le \varphi < \pi/2$) and H-aggregates ($\varphi = \pi/2$). For the cases where $\varphi = 0$ and $\pi/2$, the transition energies and the transition moments for the *m*th exciton state are (McConnell, 1961; Lin, 1989; Buck and Struve, 1996):

$$\tilde{\nu}_m = \tilde{\nu}_{mon} + 2\beta \cos\left(\frac{m\pi}{N+1}\right) \tag{2}$$

$$\mu_m = \left(\frac{2}{N+1}\right)^{1/2} \sum_n \mu_{mon} \sin\left(\frac{m \cdot n \cdot \pi}{N+1}\right) \tag{3}$$

where the summation is over all N exciton coupled states of the aggregate. Equations 2 and 3 were derived by making two important assumptions (Alden et al., 1992; Lin, 1989; McConnell, 1961; Somsen et al., 1996): 1) the monomer energy and the monomer transition moment are not affected by interactions with other monomers in the aggregate; and 2) only nearest-neighbor interactions contribute to the coupling matrix element β, which is written as (Somsen et al., 1996):

$$\beta = \frac{|\mu_{mon}|^2}{4\pi\epsilon_0\eta^2 R^3}(1 - 3\cos\theta) \tag{4}$$

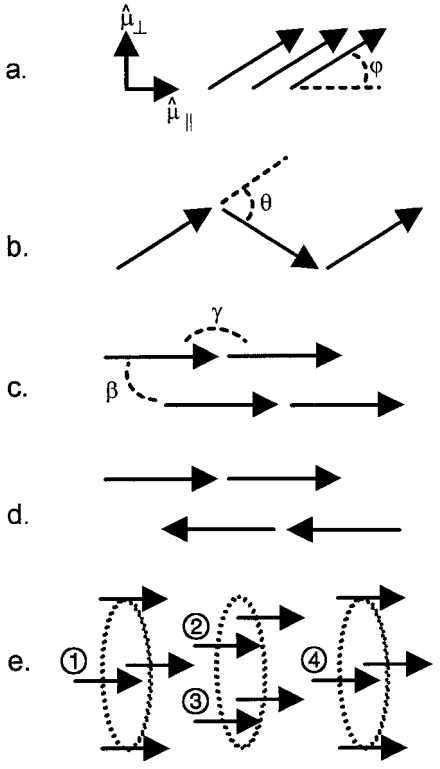

FIGURE 1 Schematic representation of the exciton-coupled systems described by our theory. (*a*) "Linear" aggregate, where the slip angle φ varies from 0 (J-aggregate) to $\pi/2$ (H-aggregate); (*b*) "zigzag" aggregate; (*c*) in-phase double stranded aggregate, where the arrows denote the designations given to the intra-strand (γ) and inter-strand (β) coupling constants; (*d*) out-of-phase double stranded aggregate; (*e*) cylindrical aggregate, where the pigments facing the front of the object are numbered. The interactions between pigments 1 and 2 and 1 and 3 are designated by β; the interaction between pigments 1 and 4 is designated as γ. All other interaction energies are obtained by symmetry.

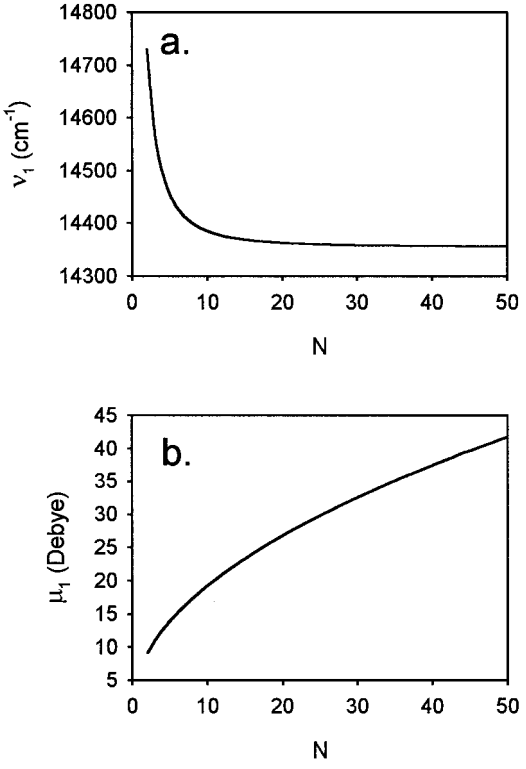

FIGURE 2 Dependence of (*a*) $\tilde{\nu}_1$ and (*b*) μ_1 on aggregate size *N*. Parameters used in the calculation are $\tilde{\nu}_{mon}$ = 15,106 cm^{-1}, μ_{mon} = 6.5 Debye, β = 400 cm^{-1}.

In Eq. 4, ϵ_o is the permittivity of free space, η is the refractive index of the medium, μ_{mon} is the transition moment of the monomer, R is the distance between nearest neighbors in the aggregate, and θ is the angle between monomer transition moment vectors in the aggregate. For a "linear" aggregate (Fig. 1 *a*), $\theta = 0$; for a "zigzag" aggregate (Fig. 1 *b*), $\theta \neq 0$.

For a J-aggregate the exciton coupling constant β is negative, which leads to red-shifts in the spectrum relative to the monomer. By contrast, $\beta > 0$ for H-aggregates, with resultant blue-shifts in the spectrum. Equations 2 and 3 also apply to a helical aggregate of any pitch or diameter where the monomer transition dipoles are aligned with the parallel axis of the helix.

For the calculations in this document we chose monomer parameters that correspond closely to those of the $Q_y(0-0)$ band of chlorophyll *a* (λ_{mon} = 662 nm, μ_{mon} = 6.5 Debye). Fig. 2 illustrates the size dependence of $\tilde{\nu}_1$ and μ_1 for a J-aggregate with $\beta = -400$ cm^{-1}. We observe (see also Alden et al., 1992) that, for large N, $\tilde{\nu}_1$ reaches a limiting value of $\tilde{\nu}_{mon} + 2\beta$ and that μ_1 varies linearly with N. We have chosen a value of β to yield a limiting $\tilde{\nu}_1$ of 699 nm, which is the transition wavelength for the largest aggregate of chlorophyll *a* formed in a 9:1 formamide/water system (de Paula et al., 1995). Although the consequences of Eqs. 2 and 3 are described with a specific numerical example, the calculations still provide useful qualitative insight that may be used to predict the behavior of any exciton-coupled aggregate.

For the remaining geometries, the general approach is to write the Hamiltonian matrix for the aggregate. The diagonal elements are equal to the monomer resonance frequencies and the off-diagonal elements reflect couplings between pigments.

For the double-stranded aggregates (Fig. 1, *c* and *d*), we define two coupling constants: one for intrastrand interactions (γ) and another for interstrand interactions (β). For example, the Hamiltonian for a tetramer is:

$$\begin{pmatrix} \tilde{\nu}_{mon} & \beta & \gamma & 0 \\ \beta & \tilde{\nu}_{mon} & \beta & \gamma \\ \gamma & \beta & \tilde{\nu}_{mon} & \beta \\ 0 & \gamma & \beta & \tilde{\nu}_{mon} \end{pmatrix} \quad (5)$$

Diagonalization of the matrix gives the transition energies and wavefunctions for the exciton split states. The transition moment for the lowest energy transition is calculated from the wavefunction of the first excited state (Eq. 6)

by Eq. 7:

$$\Phi = \sum_{j=1}^{N} C_j \phi_j \tag{6}$$

$$\mu = \mu_{mon} \cdot \left(\sum_{j=1}^{N} C_j \right) \tag{7}$$

Two alignments of the double-stranded aggregates were investigated: 1) the transition dipoles all point along the same direction (in-phase case, Fig. 1 *c*), and 2) the transition dipoles of the one strand point in the opposite direction of the transition dipoles in the other strand (out-of-phase, Fig. 1 *d*). Mathematically, this is equivalent to letting $\beta > 0$ and $\gamma < 0$.

Somsen et al. (1996) and Buck and Struve (1996) considered the effect of exciton coupling on the absorption spectra of several cylindrical aggregates. For simplicity, we consider here only the arrangement described in Fig. 1 *e*: stacks of N_2 rings, each with N_1 pigments, with each ring rotated with respect to its neighbors by a pitch angle of $2\pi/N_1$. We consider only nearest-neighbor interactions. Given the interpenetrating nature of the arrangement, each pigment interacts only with pigments that are diagonally above and below it. These couplings are reminiscent of those found in "slipped" J-aggregates (Fig. 1 *a*, $0 < \varphi < \pi/2$). Hence, the interaction energies β and γ are negative. The Hamiltonian for a three-ring cylinder, each with four pigments, is given below. The transition energies and moments are calculated as above for double-stranded aggregates (Eqs. 6 and 7).

$$\begin{pmatrix}
\nu_{mon} & 0 & 0 & 0 & \beta & \beta & 0 & 0 & \gamma & 0 & 0 & 0 \\
0 & \nu_{mon} & 0 & 0 & 0 & \beta & \beta & 0 & 0 & \gamma & 0 & 0 \\
0 & 0 & \nu_{mon} & 0 & 0 & 0 & \beta & \beta & 0 & 0 & \gamma & 0 \\
0 & 0 & 0 & \nu_{mon} & \beta & 0 & 0 & \beta & 0 & 0 & 0 & \gamma \\
\beta & 0 & 0 & \beta & \nu_{mon} & 0 & 0 & 0 & \beta & \beta & 0 & 0 \\
\beta & \beta & 0 & 0 & 0 & \nu_{mon} & 0 & 0 & 0 & \beta & \beta & 0 \\
0 & \beta & \beta & 0 & 0 & 0 & \nu_{mon} & 0 & 0 & 0 & \beta & \beta \\
0 & 0 & \beta & \beta & 0 & 0 & 0 & \nu_{mon} & \beta & 0 & 0 & \beta \\
\gamma & 0 & 0 & 0 & \beta & 0 & 0 & \beta & \nu_{mon} & 0 & 0 & 0 \\
0 & \gamma & 0 & 0 & \beta & \beta & 0 & 0 & 0 & \nu_{mon} & 0 & 0 \\
0 & 0 & \gamma & 0 & 0 & 0 & \beta & 0 & 0 & 0 & \nu_{mon} & 0 \\
0 & 0 & 0 & \gamma & 0 & 0 & \beta & \beta & 0 & 0 & 0 & \nu_{mon}
\end{pmatrix} \tag{8}$$

We have calculated the size dependence of $\tilde{\nu}_1$ for the cases in Fig. 1, *c*–*e* and quote only the results for large *N*. The double-stranded aggregates have a limiting value of $\tilde{\nu}_1 = \tilde{\nu}_{mon} + 4\beta$. The cylindrical aggregates as described have a limiting value of $\tilde{\nu}_1 = \tilde{\nu}_{mon} + 6\beta$ if $\beta = \gamma$. Also, in both cases the interactions lead to red-shifts in the absorption spectrum of the aggregate relative to that of the monomer ($\beta < 0$). However, the cylindrical and double-stranded aggregates are red-shifted more extensively than J-aggregates with the same *N* and β.

Calculation of scattering cross-sections in exciton-coupled systems

We will first describe the calculation of polarizabilities and scattering cross-sections for those cases where the transition dipole moment vector and polarizability tensor have only one component. This corresponds to all of the geometries in Fig. 1, except for the "slipped" J-aggregates, for which $0 < \varphi < \pi/2$. We may then calculate just one value of the polarizability.

We have made the following assumptions in our calculations. First, we allow only a single excited state of the monomer to contribute to the polarizability around the lower energy absorption frequency. Second, we assume that neither hyperchromism nor hypochromism is significant in these model aggregates.

The quantum mechanical expressions for the real and imaginary parts of the polarizability are given below for a system where the dipole moment vector has one component (Barron, 1976):

$$\mathrm{Re}\ \alpha(\tilde{\nu}) = \frac{1}{2\pi\epsilon_o hc} \sum_m \frac{(\tilde{\nu}_m^2 - \tilde{\nu}^2)\tilde{\nu}_m}{(\tilde{\nu}_m^2 - \tilde{\nu}^2)^2 + \tilde{\nu}^2\Gamma_m^2} |\mu_m|^2 \tag{9}$$

$$\mathrm{Im}\ \alpha(\tilde{\nu}) = \frac{1}{2\pi\epsilon_o hc} \sum_m \frac{\tilde{\nu}\tilde{\nu}_m\Gamma_m}{(\tilde{\nu}_m^2 - \tilde{\nu}^2)^2 + \tilde{\nu}^2\Gamma_m^2} |\mu_m|^2 \tag{10}$$

where $\tilde{\nu}_m$ and μ_m are defined as before and Γ_m is the spectral linewidth. The scattering (C_{sca}) and absorption (C_{abs}) cross-sections follow directly from Eqs. 9 and 10 and the definitions (Pasternack and Collings, 1995):

$$C_{sca} = \frac{8}{3}\pi^3\tilde{\nu}^4[\mathrm{Re}(\alpha)^2 + \mathrm{Im}(\alpha)^2] \tag{11}$$

$$C_{abs} = 2\pi\tilde{\nu}\,\mathrm{Im}(\alpha) \tag{12}$$

We have chosen units for the parameters and variables in Eqs. 9–12 so that the polarizabilities are expressed in cm^3/molecule and the cross-sections in cm^2/molecule.

Our exciton coupling calculations confirm earlier results by Alden et al. (1992), who showed that the transition to the first exciton state of the aggregate is far stronger than transitions to other exciton states. Consequently, $\mathrm{Im}(\alpha)$ peaks and $\mathrm{Re}(\alpha)$ vanishes at ν_1. This leads to the prediction that C_{sca} peaks at ν_1, which is the resonance light scattering effect. The next two sections illustrate further the behavior of C_{sca} and C_{abs} for the "linear" aggregate case (Fig. 1 *a*, $\theta = \varphi = 0$).

Dependence of RLS intensity on aggregate size

Fig. 2 suggests that $\tilde{\nu}_1$ decreases sharply and μ_1 increases somewhat less sharply with size until $N \approx 25$. For $N > 25$, $\tilde{\nu}_1$ approaches the limiting value of $\tilde{\nu}_{mon} + 2\beta$, while μ_1 continues to increase. These results have two important consequences. First, using the position of the strongest absorption band to determine the size of a large J-aggregate (Horng and Quitevis, 1993) may lead to errors. Second, $C_{sca}(\tilde{\nu}_1)$ does not begin to depend strongly on size until $N > 25$ (Fig. 3).

Dependence of RLS intensity on electronic coupling

It is important to consider four features of our model when evaluating the effect of electronic coupling on C_{sca} of linear J- or H-aggregates ($\theta = 0$). First, Eq. 4 suggests that two parameters modulate electronic coupling very efficiently in these aggregates: the interchromophore distance R and the monomer transition moment μ_{mon}. Second, we conclude from Eqs. 2 and 3 that changes in β modulate $\tilde{\nu}_1$ only; μ_1 is independent of β at this level of approximation. Third, the polarizability scales with the volume of the aggregate (van de Hulst, 1981). Our calculations confirm that α^2 does indeed increase with R regardless of the sign and magnitude of the β parameter (data not shown). Lastly, $C_{sca}(\tilde{\nu}_1)$ depends both on the square of the volume of the aggregate and on the fourth power of the absorption frequency $\tilde{\nu}_1$ (Eq. 11). These principles facilitate the interpretation of the data in Fig. 4, which shows the dependence of $C_{sca}(\tilde{\nu}_1)$ on R and μ_{mon} for "linear" aggregates with $N = 100$.

Fig. 4 *a* shows the effect of changes in R on $C_{sca}(\tilde{\nu}_1)$. For a J-aggregate ($\beta < 0$), $C_{sca}(\tilde{\nu}_1)$ is not strongly dependent on R, but does increase monotonically with R. The data are consistent with the expectation that C_{sca} should increase with the size of the aggregate. In this case both the α^2 and $\tilde{\nu}_1^4$ terms work together to give the observed behavior. By increasing the R value, we cause $|\beta|$ to decrease, which in turn enhances the $\tilde{\nu}_1^4$ term. Moreover, increasing R also increases the length of the aggregate and thus enhances the α^2 term. Therefore, $C_{sca}(\tilde{\nu}_1)$ increases with R even though the strength of electronic coupling, as measured by the magnitude of β, decreases.

Fig. 4 *a* also shows that $C_{sca}(\tilde{\nu}_1)$ decreases with increasing R for an H-aggregate ($\beta > 0$). The data illustrate the interaction between the $\tilde{\nu}_1^4$ and α^2 terms in the expression for $C_{sca}(\tilde{\nu}_1)$ (Eq. 11). Increasing R results in a decrease in $|\beta|$ and attendant decreases in $\tilde{\nu}_1$. Even though α^2 does increase with R (data not shown), the $\tilde{\nu}_1^4$ term predominates, leading to the counterintuitive result that the magnitude of $C_{sca}(\tilde{\nu}_1)$

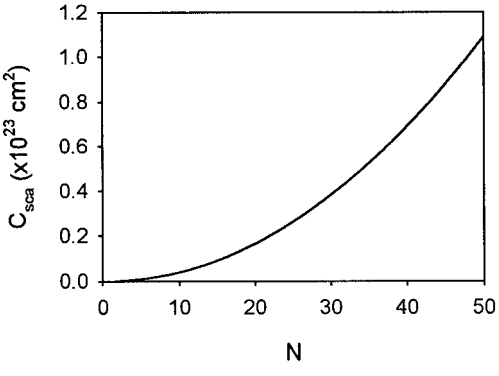

FIGURE 3 Dependence of C_{sca} at the resonance frequency $\tilde{\nu}_1$ on aggregate size N. Parameters used in the calculation as for Fig. 2, with the addition that $\Gamma = 400\ cm^{-1}$. The specific values of Γ and β were chosen so that the width and position of the Q_y band of chlorophyll *a* aggregates (de Paula et al., 1995; Fig. 7) would be approximated by the calculation.

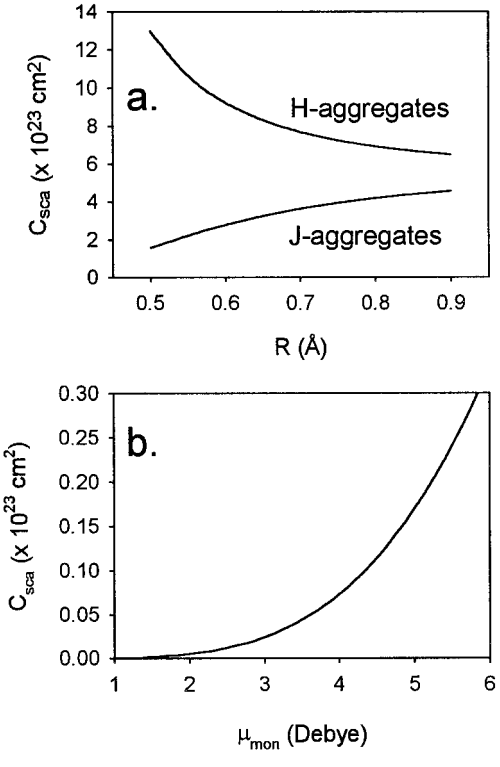

FIGURE 4 (*a*) Dependence of C_{sca} at the resonance frequency $\tilde{\nu}_1$ on the interchromophore distance R in J- and H-aggregates ($N = 100$, $\mu_{mon} = 6.5$ Debye). (*b*) Dependence of C_{sca} at the resonance frequency $\tilde{\nu}_1$ on μ_{mon} ($N = 100$, $R = 0.86$ nm) in a J-aggregate. All other parameters are as in Figs. 2 and 3.

is inversely proportional to the value of R. However, in this geometry we observe that C_{sca} does increase with the strength of electronic coupling.

Fig. 4 *b* shows the effect of changes in μ_{mon} on $C_{sca}(\tilde{\nu}_1)$. According to Eqs. 2–4, this affects μ_m, β, and $\tilde{\nu}_m$. For a J-aggregate with given $\tilde{\nu}_{mon}$, R, θ, and N, $C_{sca}(\tilde{\nu}_1)$ increases strongly with μ_{mon}. Qualitatively similar results are obtained for H-aggregates (data not shown). The value of μ_{mon} may be changed either by changing the chemical composition of the aggregate or through intramolecular interactions that affect the electronic structure of the monomer in the aggregate (Ohno et al., 1993).

Dependence of RLS intensity on aggregate geometry

Table 1 compares $C_{sca}(\tilde{\nu}_1)$ for aggregates with different geometries but the same number of monomers ($N = 100$) and coupling constants ($\beta = \gamma = -400$ cm^{-1} for all cases except for H-aggregates, where $\beta = 400$ cm^{-1}). We find that $C_{sca}(\tilde{\nu}_1)$ is largest for H- and J-aggregates and smallest for cylindrical aggregates.

Among the double-stranded aggregates, the in-phase alignment results in far greater C_{sca} when compared to the out-of-phase alignment. Among the cylindrical aggregates, short cylinders with many monomers per ring are better scatterers than long cylinders with few monomers per ring.

The dependence of $C_{sca}(\tilde{\nu}_1)$ on aggregate geometry may be understood in terms of the above discussion on J-aggregates. Cylindrical and double-stranded aggregates show larger red-shifts in their absorption spectra than do J-aggregates. However, the magnitude of μ_1 depends only on the number of monomers bound in the aggregate, not on geometry. Therefore, the lower values of $\tilde{\nu}_1$ in the cylinders and double strands result in lower scattering cross-sections for a given N, relative to the predictions for J-aggregates.

Calculation of RLS depolarization ratios of J-aggregates

Stanton et al. (1981), Strommen (1992), and Barron (1976) summarize the theory that leads to the calculation of depolarization ratios in resonance Rayleigh and Raman scattering. Depolarization of the incident light is a result of anisotropy in the molecular polarizability. Hence, α may be described as a tensor; it is in fact a complex symmetric tensor.

TABLE 1 Resonance light scattering cross-sections for model chromophore aggregates in a variety of geometries ($\lambda_{mon} = 662$ nm, $\mu_{mon} = 6.5$ Debye, $\theta = \varphi = 0$, $\beta = \gamma = -400$ cm^{-1}, $N = 100$)

Geometry	λ_{max} (nm)	$C_{sca}(\lambda_{max})$ ($\times 10^{23}$ cm^2)
Double strands (out-of-phase)	740	0.06
Cylinders ($N_1 = 5$, $N_2 = 20$)	784	2.21
Cylinders ($N_1 = 10$, $N_2 = 10$)	776	2.41
Cylinders ($N_1 = 20$, $N_2 = 5$)	755	3.02
Double strands (in-phase)	740	3.36
J-aggregates	699	4.38
H-aggregate	628	6.69

The general form of the depolarization ratio $\rho_V(90)$ for incident vertically polarized light and a 90° scattering geometry is (Barron, 1976; Strommen, 1992):

$$\rho_V(90) = \frac{3|\gamma_s|^2 + 5|\gamma_{as}|^2}{45|\bar{\alpha}|^2 + 4|\gamma_s|^2} \tag{13}$$

where the trace of the polarizability tensor, the symmetric anisotropic, and antisymmetric anisotropic tensor invariants are given respectively by:

$$\bar{\alpha}(\tilde{\nu}) = \frac{1}{3}(\alpha_{xx} + \alpha_{yy} + \alpha_{zz}) \tag{14}$$

$$|\gamma_s|^2 = \frac{1}{2}[(\alpha_{xx} - \alpha_{yy})^2 + (\alpha_{yy} - \alpha_{zz})^2 + (\alpha_{zz} - \alpha_{xx})^2] + \frac{3}{4}[(\alpha_{xy} - \alpha_{yx})^2 + (\alpha_{yz} - \alpha_{zy})^2 + (\alpha_{zx} - \alpha_{xz})^2] \tag{15}$$

$$|\gamma_{as}|^2 = \frac{3}{4}[(\alpha_{xy} - \alpha_{yz})^2 + (\alpha_{yz} - \alpha_{zy})^2 + (\alpha_{zx} - \alpha_{xz})^2] \tag{16}$$

In resonance Rayleigh scattering, the scattering tensor is symmetric and γ_{as} is zero (Barron, 1976). Therefore,

$$\rho_V(90) = \frac{3|\gamma_s|^2}{45|\bar{\alpha}|^2 + 4|\gamma_s|^2} \tag{17}$$

It is simple to calculate $\rho_V(90)$ for three limiting cases: 1) an aggregate with a spherically symmetric tensor ($\alpha_{xx} = \alpha_{yy} = \alpha_{zz}$) has $\rho_V(90) = 0$; 2) an aggregate with one nondegenerate excited state ($\alpha_\parallel \gg \alpha_\perp$) has $\rho_V(90) = 1/3$; and 3) an aggregate with a degenerate excited state ($\alpha_\parallel \ll \alpha_\perp$) has $\rho_V(90) = 1/8$. Nondegenerate excited states are expected for the idealized J-type, H-type, cylindrical, and double stranded aggregates described previously ($\varphi = 0$) because the net transition dipole moment vector has one component in the axis system defined by the molecular frame. However, the limiting values for the depolarization ratio may be observed only rarely. For example, $\rho_V(90) = 1/3$ is predicted for excited states where $\alpha_\parallel/\alpha_\perp > 1000$. This may only occur in aggregates with a high degree of long-range order.

Fig. 5 shows the variation in $\rho_v(90)$ with $\alpha_\parallel/\alpha_\perp$. The data point out some limitations in the use of $\rho_V(90)$ for the characterization of symmetric top excited states. Namely, two geometries are consistent with each value of $\rho_V(90)$ below 1/8 and above 0. Most striking is the fact that a $\rho_V(90)$ value of 1/8 is consistent with both $\alpha_\parallel/\alpha_\perp = 0$ and $\alpha_\parallel/\alpha_\perp = 4$. Consequently, only if $\rho_V(90) > 1/8$ or $\alpha_\parallel/\alpha_\perp > 4$ can the data be described by a unique geometry.

The preceding analysis applies to any scatterer, including monomeric species. However, the emphasis here is on ag-

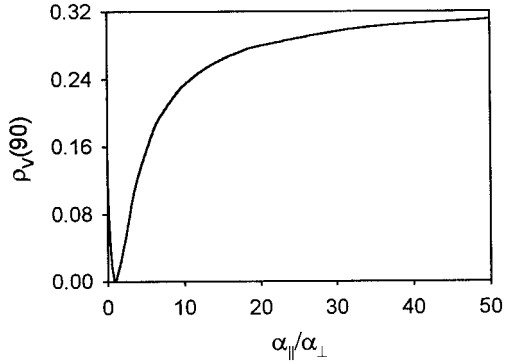

FIGURE 5 Variation of $\rho_v(90)$ with $\alpha_\parallel/\alpha_\perp$. The limiting value of $\rho_V(90) = ⅓$ is only reached for $\alpha_\parallel/\alpha_\perp > 1000$.

gregates. The simplest geometry that yields non-zero values of $\alpha_\parallel$ and $\alpha_\perp$ is that depicted by Fig. 1 *a* for $0 < \varphi < \pi/2$. The parallel and perpendicular components of the transition dipole moment vector for the *m*th exciton state of these "slipped" J-aggregates are given by Pearlstein (1991):

$$\mu_{m\parallel} = \left(\frac{2}{N+1}\right)^{1/2} \sum_n \mu_{mon} \cdot \cos\varphi \cdot \sin\left(\frac{m \cdot n \cdot \pi}{N+1}\right) \quad (18)$$

$$\mu_{m\perp} = \left(\frac{2}{N+1}\right)^{1/2} \sum_n \mu_{mon} \cdot \sin\varphi \cdot \sin\left(\frac{m \cdot n \cdot \pi}{N+1}\right) \quad (19)$$

From these, the parallel and perpendicular components of the polarizability tensor are calculated with Eqs. 9 and 10. The depolarization ratio then follows from Eq. 17. Fig. 6 shows the dependence of $\rho_v(90)$ at $\tilde{\nu}_1$ on the "slip" angle φ. As expected from the analysis given above, $⅛ \leq \rho_v(90) \leq ⅓$. The curve is symmetrical around $\varphi = \pi/4$, so that $\rho_V(90)$ rises to ⅓ at $\varphi = \pi/2$.

The treatment above is not limited to the geometry of Fig. 1 *a*. Any aggregate with non-zero values of $\alpha_\parallel$ and $\alpha_\perp$ will yield results that can be interpreted with Fig. 6. Examples include: 1) a helical or cylindrical aggregate where the monomer transition dipoles point away from the major axis by an angle φ; and 2) a double strand consisting of two interacting slipped J-aggregates.

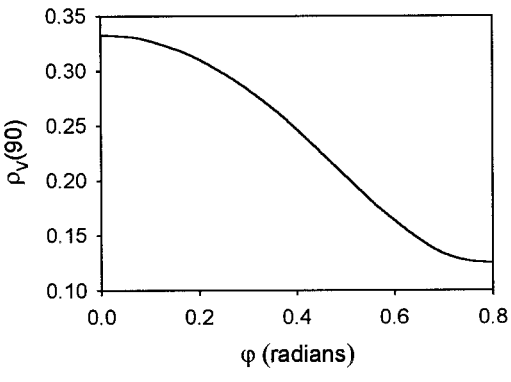

FIGURE 6 Dependence of $\rho_v(90)$ at $\tilde{\nu}_1$ on the "slip" angle φ. The parameters used in the calculation were as in Fig. 2, with $N = 100$.

RESULTS

Table 2 summarizes the depolarization ratios for aggregates of $H_4TPPS_4^{2-}$ at pH 0.5, CuP_{agg}^{2+} in 0.2 M NaCl and on DNA, and chlorophyll *a* in formamide/buffer (pH 6.8). The data were obtained at or very near their respective resonance wavelengths, with either a spectrofluorimeter or with a laser light scattering apparatus, as described in the Materials and Methods section. We were unable to obtain laser light scattering data at 699 nm because our mixed gas ion laser does not have emission lines near that wavelength. The good agreement between the fluorimeter and laser light scattering apparatus demonstrates that Eq. 1 is valid. Therefore, reliable RLS depolarization ratios may be obtained with instrumentation that is both readily available and relatively inexpensive.

Fig. 7 shows that $\rho_V(90)$ varies with wavelength. We have chosen to show this behavior for the 699 nm band of chlorophyll *a* aggregates because, unlike the Soret band (also known as the B band), the Q_y transition of chlorophyll *a* is pure (van Zandvoort et al., 1995). As a result, the dispersion of $\rho_V(90)$ within the 699 nm band is not likely to be an artifact of spectral congestion that may occur from closely spaced x- and y-polarized transitions.

The data in Fig. 7 are fully consistent with the theoretical treatment of Stanton et al. (1981) for symmetric tops. Dispersion of $\rho_V(90)$ arises from the frequency dependence of the molecular polarizability (Eqs. 9 and 10). At frequencies far below the resonance frequency, the depolarization ratio is dictated by the system's static polarizability tensor, which, in turn, depends on the structure of the system's ground state. At the resonance frequency, the depolarization ratio depends on the polarizability induced by the electronic transition. The value of $\rho_V(90)$ is expected to increase with increasing frequency, reaching a plateau near the resonance frequency (Stanton et al., 1981). Beyond resonance, the depolarization ratio rises and can reach a maximum value of ¾ at a wavelength where the tensor's trace ($\bar{\alpha}$) vanishes (Eq. 17). For every symmetric top, there is a wavelength

TABLE 2 Depolarization ratios at resonance for some porphyrin and chlorophyll aggregates

Sample	λ (nm)	$\rho_V(90)$
$H_4TPPS_4^{2-}$ at pH 0.5	488	0.17*#
CuP_{agg}^{2+}		
in 0.2 M NaCl	450	0.13*
	454	0.15#
on DNA	454	0.20*
	454	0.16#
Chlorophyll *a* in formamide/buffer (pH 6.8)	469	0.23*
	468	0.22#
	699	0.32*

*Measured with a spectrofluorimeter.
#Measured with a laser light scattering apparatus.

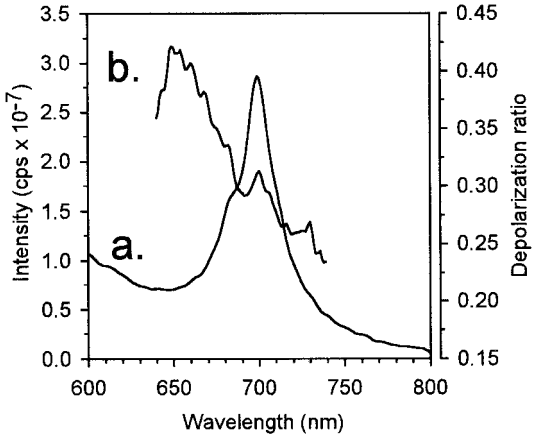

FIGURE 7 Dispersion of $\rho_V(90)$ within the RLS spectrum of chlorophyll *a* aggregated in formamide/buffer. (*a*) RLS spectrum of the chlorophyll *a* aggregate in the Q_y region; (*b*) dependence of $\rho_V(90)$ with wavelength in the Q_y region.

(away from resonance) at which this condition is met. At higher frequencies still, the depolarization ratio goes to zero. Consequently, $\rho_V(90)$ measured at the resonance frequency reports directly on the structure of the aggregate's excited state.

DISCUSSION

Factors that determine intensity in resonance light scattering spectra

The calculations presented above lead to predictions of which molecular systems are amenable to analysis by RLS spectroscopy. However, it is important to discuss the limitations of the model before moving on to predictions.

Our calculations do not include charge-resonance (CR) and charge-transfer (CT) interactions. Thompson et al. (1991) have argued that such interactions contribute importantly to the position and intensity of the absorption spectrum of the bacteriochlorophyll *b* dimer in the reaction center of *Rhodopseudomonas viridis*. For example, both CT and CR enhance the extent of red-shift in the aggregate's absorption spectrum relative to the monomer spectrum. Hence, CR and CT interactions are likely to modulate RLS intensities as well. However, we have chosen the simplest exciton-coupling model in order to minimize the number of adjustable parameters in the calculations. We believe that as long as the simple model is used appropriately and consistently we can gain qualitative insight into the RLS phenomenon. Our future efforts at understanding not only RLS intensities but also the electronic structure of porphyrin and chlorophyll aggregates will feature basis sets where CR and CT will be included explicitly.

Alden et al. (1992) point out that the exciton coupling calculations summarized by Eqs. 2–8 are valid for aggregate sizes that are considerably smaller than the resonance wavelength. For chlorophyll aggregates with moderately long resonance wavelengths ($\lambda > 660$ nm), the calculations may be taken to be valid up to $N \sim 100$, which translates to an effective length of ~200 nm for chlorophyll aggregates. As the aggregate size becomes very large, two effects are likely to occur: 1) the diagonal elements of the exciton coupling Hamiltonian will deviate from $\tilde{\nu}_{mon}$, and 2) the monomer transition moments will deviate from μ_{mon}. A charge resonance interaction between the Soret and Q states of the monomers is among the mechanisms that can bring about these changes (Ohno et al., 1993).

As a result of these constraints, our calculations of scattering cross-sections are ideally suited for investigation of relatively small aggregates. To this end, the data show that the scattering cross-section at the resonance frequency increases with size of an exciton-coupled aggregate of chromophores. However, the dependence is not simple and C_{sca} does not depend strongly on size until $N > 25$. These results explain some experimental observations concerning resonance light scattering spectroscopy: 1) monomers, dimers, and trimers of porphyrins do not show enough RLS to overcome absorption effects in the spectrum (Anglister and Steinberg, 1979; Stanton et al., 1981; Pasternack et al., 1993, 1994; de Paula et al., 1995; Borissevitch et al., 1997); and 2) the same is true for chlorophyll-binding proteins, such as the 47-kDa antenna protein of spinach photosystem II, which binds as many as 25 chlorophylls (data not shown).

Preliminary measurements of the size of $H_4TPPS_4^{2-}$ at low pH indicate that $N \approx 10^4$-10^5 (Pasternack, Gibbs, and Collings, unpublished results). Assuming that $N = 10^5$ and that the aggregate is roughly a cylinder (Ohno et al., 1993) with a radius corresponding to the radius of a tetraphenylporphine molecule [~0.2 nm; see Tran-Thi et al. (1992) for a justification], we estimate that the length of the aggregate is roughly 16 μm. We conclude from our calculations and observations to date that the aggregate must be very large in order to exhibit RLS spectra that are essentially free of absorption effects. A more exact determination of the threshold beyond which RLS overcomes absorption in synchronous luminescence measurements requires the characterization of systems where aggregate size may be controlled in the range $10^2 < N < 10^5$. Such experiments are being conducted in our laboratories.

Our results suggest that in addition to size two molecular parameters are important determinants of RLS intensity: electronic coupling and aggregate geometry. However, it is not always prudent to consider size, geometry, and electronic coupling as completely independent factors. For example, the resonance scattering cross-section depends on the mechanism through which coupling electronic coupling is modulated, as shown by Fig. 4. On the one hand, the scattering cross-section may be increased by increasing the monomer transition moment (Fig. 4 *b*). This may occur via charge resonance interactions between monomers which in turn may be facilitated by changes in the size and geometry of the aggregate (Ohno et al., 1993). On the other hand, changes in interchromophore distance can either increase or

decrease the scattering cross-section in a manner that is dependent on the geometry of the aggregate (Fig. 4 *a*).

Depolarized RLS as a probe of structure

Our theory predicts that the value of $\rho_v(90)$ depends only on the ratio of the principal values of the polarizability tensor at the resonance frequency. Therefore, the depolarization ratio reports on the geometry of the excited state of the aggregate, regardless of its size. To this extent, our calculations of $\rho_v(90)$ do not suffer from the limitations described above for the calculations of absolute values of C_{sca}.

The $H_4TPPS_4^{2-}$ aggregate at pH 0.5 has $\rho_v(90) = 0.17$ at 488 nm. From Fig. 5 we calculate $\alpha_\parallel/\alpha_\perp = 5.6$. Based on electronic absorption, fluorescence, and resonance Raman measurements, Ohno et al. (1993), Maiti et al. (1995), and Akins et al. (1996) have proposed that this system resembles the slipped J-aggregate of Fig. 1 *a*, but the data did not allow for a determination of the slip angle φ. From our depolarized RLS measurement and from Eqs. 17–19, we calculate a value of $\varphi = 33°$ or $56°$.

The self-assembled aggregate of CuP_{agg}^{2+} in 0.2 M NaCl has $\rho_V(90) = 0.13$ at 450 nm, which corresponds to $\alpha_\parallel/\alpha_\perp = 4.2$ (Fig. 5). This system also has spectral properties that suggest a J-aggregate (Pasternack et al., 1991). By applying the same rationale used above for the $H_4TPPS_4^{2-}$ aggregates, we calculate $\varphi = 41°$ or $49°$. The CuP_{agg}^{2+}/DNA system has $\rho_V(90) = 0.20$ at 454 nm, which corresponds to $\alpha_\parallel/\alpha_\perp = 7.2$. Electronic absorption and RLS data suggest that the porphyrin forms a helical aggregate on the DNA template (Pasternack et al., 1991, 1993). Our depolarized RLS data are consistent with this hypothesis and further suggest that the porphyrin transition dipoles point away from the DNA helix axis by an angle of $29°$ or $61°$.

The chlorophyll *a* aggregate in formamide/phosphate buffer (pH 6.8) has $\rho_V(90)$ values of 0.23 and 0.32 at 469 nm (Soret band) and 699 nm (Q_y band), respectively. These correspond to $\alpha_\parallel/\alpha_\perp$ values of 9.7 (Soret band) and 85 (Q_y band). Spectroscopic data on both chlorophyll *a* and bacteriochlorophyll *a* in aqueous formamide systems suggest that they self-assemble into a J-type aggregate with a helical structure (Scherz et al., 1991; de Paula et al., 1995). Our depolarized RLS data are consistent with either a slipped J-aggregate or with an anisotropic helical aggregate.

The data also suggest that the transition dipoles giving rise to the Soret band are "slipped" by $\varphi = 25°$ or $65°$, whereas the Q_y dipoles are "slipped" by $\varphi = 9°$ or $81°$. Whereas either value for the slip between the Soret dipole and the aggregate axis is possible, we must exclude $81°$ as a possibility for the slip angle between the Q_y dipole and the aggregate axis. This is because between the two possibilities only a slip angle of $9°$ is consistent with the observed red-shift of the Q_y transition upon aggregation. A slip angle of $81°$ is consistent with an H-aggregate structure and would result in blue shifts in the Q_y transition upon aggregation.

Fig. 8 *b* proposes a model that incorporates our RLS data and the known orientations of the B_x, B_y, and Q_y transitions of monomeric chlorophyll *a* with respect to its molecular axes (van Zandvoort et al., 1995). Given that the angle between the B_y and Q_y vectors is $9°$ and that we predict $\varphi = 9°$ for the angle between the aggregate axis and the monomer Q_y vector, we expect values of $18°$ and $62°$ for the slip angles between the aggregate axis and the monomer B_y and B_x vectors, respectively. This is in reasonable agreement with $\varphi = 25°$ and $65°$ that we measured for the slip angle between the Soret transition moment vector and the aggregate axis.

The packing geometry derived from our RLS measurements is similar to that observed by x-ray diffraction in crystals of methyl chlorophyllide *a* (Kratky and Dunitz, 1977). Taken together, our RLS data and previous crystallographic data indicate that ring-ring interactions are important factors in the formation of chlorophyll *a* aggregates (at least in the aqueous formamide solvent system). The stacking arrangement shown in Fig. 8 *b* also allows for the phytyl chains of chlorophyll *a*, which are covalently attached to ring IV (Fig. 8 *a*), to participate in hydrophobic interactions. These interactions provide an additional driving force for aggregation.

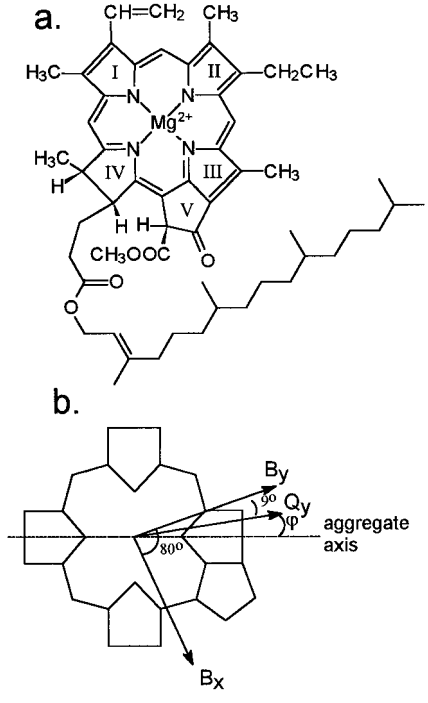

FIGURE 8 (*a*) Structure of chlorophyll *a* showing the ring numbering system used in the text. (*b*) Proposed alignment of the chlorophyll *a* monomer transition moments with respect to the long axis of the aggregate. The dashed line (the "aggregate axis") represents the direction along which the macrocycles aggregate, with each macrocycle having the orientation shown in the figure. Only one monomer is shown.

CONCLUSIONS

Our data indicate that depolarized resonance light scattering is a powerful technique for the study of porphyrin and chlorophyll *a* aggregates. A simple determination of $\rho_V(90)$ with a commercial fluorimeter yields in fluid solution the same structural information that would only be accessible through linear dichroism studies in rigid or oriented systems. Our application of the technique to chlorophyll *a* aggregates led to a model (Fig. 8) of the alignment of the monomer units that is consistent with the crystal packing of chlorophyll *a* derivatives (Kratky and Dunitz, 1977).

Our calculations and a number of experiments by different groups indicate that the RLS technique, although highly sensitive to exciton-coupled aggregates, is limited in scope: only nanometer-to-micron-sized particles are likely to yield RLS signatures that are not affected strongly by absorption. However, this feature of the technique may be exploited in the study of a variety of biological and synthetic macromolecular systems, ranging from the light-harvesting chlorosomes of green photosynthetic bacteria (Blankenship et al., 1995) to materials for nonlinear optical applications (Schultz et al., 1990).

This work was supported by National Science Foundation grant CHE-9530707 (to J.dP., R.F.P., P.C., E.G.).

REFERENCES

Akins, D. L., H.-R. Zhu, and C. Guo. 1996. Aggregation of tetraaryl-substituted porphyrins in homogeneous solution. *J. Phys. Chem.* 100: 5420–5425.

Alden, R. G., S. H. Lin, and R. E. Blankenship. 1992. Theory of spectroscopy and energy transfer of oligomeric pigments in chlorosome antennas of green photosynthetic bacteria. *J. Lumin.* 51:51–66.

Anglister, J., and I. Z. Steinberg. 1979. Depolarized Rayleigh light scattering in absorption bands measured in lycopene solution. *Chem. Phys. Lett.* 65:50–54.

Barron, L. D. 1976. Rayleigh and Raman scattering of polarized light. *In* Molecular Spectroscopy, Vol. 4. The Chemical Society, London. 96–124.

Blankenship, R. E., J. M. Olson, and M. Miller. 1995. Antenna complexes from green photosynthetic bacteria. *In* Anoxygenic Photosynthetic Bacteria. R. E. Blankenship, M. T. Madigan, and C. E. Bauer, editors. Kluwer Academic Publishers, Dordrecht. 399–435.

Borissevitch, I. E., T. T. Tominaga, H. Imasato, and M. Tabak. 1997. Resonance light scattering study of aggregation of two water soluble porphyrins due to their interaction with bovine serum albumin. *Anal. Chim. Acta*. 343:281–286.

Buck, D. R., and W. S. Struve. 1996. Tubular exciton models for BChl *c* antennae in chlorosomes from green photosynthetic bacteria. *Photosyn. Res.* 48:367–377.

Cogdell, R. J., P. K. Fyfe, S. J. Barrett, S. M. Prince, A. A. Freer, N. W. Isaacs, P. McGlynn, and C. N. Hunter. 1996. The purple bacterial photosynthetic unit. *Photosyn. Res.* 48:55–63.

de Paula, J. C., J. H. Robblee, and R. F. Pasternack. 1995. Aggregation of chlorophyll *a* probed by resonance light scattering spectroscopy. *Biophys. J.* 68:335–341.

Fuhrhop, J.-H., O. Bindig, C. Demoulin, B. Rosengarten, and U. Siggel. 1994. Polymeric porphyrin and metalloporphyrin assemblies in bulk solution. *Macromol. Symp.* 80:63–82.

Gurioli, M., F. Bogani, S. Ceccherini, A. Vinattieri, and M. Colocci. 1996. Resonant elastic light scattering and coherence relaxation in semiconductor structures. *J. Opt. Soc. Am. B*. 13:1232–1240.

Horng, M.-L., and E. L. Quitevis. 1993. Excited-state dynamics of polymer-bound J-aggregates. *J. Phys. Chem.* 97:12408–12415.

Huang, C. Z., K. A. Li, and S. Y. Tong. 1997. Determination of nanograms of nucleic acids by their enhancement effect of the resonance light scattering of the cobalt(II)/4-[(5-chloro-2-pyridyl)azo]-1,3-diaminobenzene complex. *Anal. Chem.* 69:514–520.

Karrash, S., P. A. Bullough, and R. Ghosh. 1995. The 8.5 Å projection map of the light-harvesting complex I from *Rhodospirillum rubrum* reveals a ring composed of 16 subunits. *EMBO J.* 14:631–638.

Katz, J. J., M. K. Bowman, T. J. Michalski, and D. L. Worcester. 1991. Chlorophyll aggregation: chlorophyll/water micelles as models for in vivo long-wavelength chlorophyll. *In* Chlorophylls. H. Scheer, editor. CRC Press, Boca Raton. 211–235.

Kratky, C., and J. D. Dunitz. 1977. Ordered aggregation states of chlorophyll *a* and some derivatives. *J. Mol. Biol.* 113:431–442.

Lakowicz, J. R. 1986. Fluorescence polarization. *In* Principles of Fluorescence Spectroscopy. Plenum Press, New York. 112–154.

Lagendijk, A., and B. A. van Tiggelen. 1996. Resonant multiple scattering of light. *Phys. Repts.* 270:143–215.

Lehn, J.-M. 1995. Molecular and supramolecular devices. *In* Supramolecular Chemistry. VCH, Weinheim. 89–138.

Lin, S. 1989. Theory of photoinduced intramolecular electron transfer in condensed media. *J. Chem. Phys.* 90:7103–7113.

Ma, C. Q., K. A. Li, and S. Y. Tong. 1996. Microdetermination of proteins by resonance light scattering spectroscopy with bromphenol blue. *Anal. Biochem.* 239:86–91.

Ma, C. Q., K. A. Li, and S. Y. Tong. 1997. Microdetermination of proteins by resonance light scattering spectroscopy with tetraiodo phenol sulfonaphthalein. *Fresenius J. Anal. Chem.* 357:915–920.

Maiti, N. C., M. Ravikanth, S. Mazumdar, and N. Periasamy. 1995. Fluorescence dynamics of noncovalently linked porphyrin dimers and aggregates. *J. Phys. Chem.* 99:17192–17197.

McConnell, H. M. 1961. Intramolecular charge transfer in aromatic free radicals. *J. Chem. Phys.* 35:508–515.

McDermott, G., S. M. Prince, A. A. Freer, A. M. Hawthornthwaite-Lawless, M. Z. Papiz, R. J. Cogdell, and N. W. Isaacs. 1995. Crystal structure of an integral membrane light-harvesting complex from photosynthetic bacteria. *Nature*. 374:517–521.

Miller, G. A. 1978. Fluctuation theory of the resonance enhancement of Rayleigh scattering in absorbing media. *J. Phys. Chem.* 82:616–618.

Ohno, O., Y. Kaizu, and H. Kobayashi. 1993. J-aggregate formation of a water-soluble porphyrin in acidic aqueous media. *J. Chem. Phys.* 99: 4128–4139.

Pasternack, R. F., C. Bustamante, P. J. Collings, A. Giannetto, and E. J. Gibbs. 1993. Porphyrin assemblies on DNA studied by a resonance light scattering technique. *J. Am. Chem. Soc.* 115:5393–5399.

Pasternack, R. F., and P. J. Collings. 1995. Resonance light scattering: a new technique for studying chromophore aggregation. *Science*. 269: 935–939.

Pasternack, R. F., A. Giannetto, P. Pagano, and E. J. Gibbs. 1991. Self-assembly of porphyrins on nucleic acids and polypeptides. *J. Am. Chem. Soc.* 113:7799–7800.

Pasternack, R. F., and E. J. Gibbs. 1996. Porphyrins and metalloporphyrin interactions with nucleic acids. *In* Metal Ions in Biological Systems, Vol. 33. Probing of Nucleic Acids by Metal Ion Complexes of Small Molecules. A. Sigel and H. Sigel, editors. Marcel Dekker, New York. 367–397.

Pasternack, R. F., S. Gurrieri, R. Lauceri, and R. Purrello. 1996. Single-stranded nucleic acids as templates for porphyrin assembly formation. *Inorg. Chim. Acta*. 246:7–12.

Pasternack, R. F., K. F. Schaefer, and P. Hambright. 1994. Resonance light scattering studies of porphyrin diacid aggregates. *Inorg. Chem.* 33: 2062–2065.

Pearlstein, R. M. 1991. Theoretical interpretation of antenna spectra. *In* Chlorophylls. H. Scheer, editor. CRC Press, Boca Raton. 1047–1078.

Pullerits, T., and V. Sundström. 1996. Photosynthetic light-harvesting pigment-protein complexes: toward understanding how and why. *Acc. Chem. Res.* 29:381–389.

Scherz, A., V. Rosenbach-Belkin, and J. R. E. Fisher. 1991. Chlorophyll aggregates in aqueous solutions. *In* Chlorophylls. H. Scheer, editor. CRC Press, Boca Raton. 237–268.

Schultz, H., H. Lehmann, M. Rein, and M. Hanack. 1990. Phthalocyaninatometal and related complexes with special electrical and optical properties. *In* Structure and Bonding 74. Springer-Verlag, Berlin. 41–146.

Somsen, O. J. G., R. van Grondelle, and H. van Amerongen. 1996. Spectral broadening of interacting pigments: polarized absorption by photosynthetic proteins. *Biophys. J.* 71:1934–1951.

Stanton, S. G., R. Pecora, and B. S. Hudson. 1981. Resonance enhanced dynamic Rayleigh scattering. *J. Chem. Phys.* 75:5615–5625.

Strommen, D. P. 1992. Specific values of the depolarization ratio in Raman spectroscopy. *J. Chem. Ed.* 69:803–807.

Thompson, M. A., M. C. Zerner, and J. Fajer. 1991. A theoretical examination of the electronic structure and excited states of the bacteriochlorophyll *b* dimer from *Rhodopseudomonas viridis*. *J. Phys. Chem.* 95: 5693–5700.

Tran-Thi, T. H., J. F. Lipskier, P. Maillard, M. Momentau, J.-M. Lopez-Castillo, and J. P. Jay-Gerin. 1992. Effect of the exciton coupling on the optical and photophysical properties of face-to-face porphyrin dimers and trimer. A treatment including the solvent stabilization effect. *J. Phys. Chem.* 96:1073–1082.

van de Hulst, H. C. 1981. *In* Light Scattering by Small Particles. Dover Publications, New York. 63–66.

van Zandvoort, M. A. M., D. Wröbel, P. Lettinga, G. van Ginkel, and Y. K. Levine. 1995. The orientation of the transition dipole moments of chlorophyll *a* and pheophytin *a* in their molecular frame. *Photochem. Photobiol.* 62:299–308.